CIRP Annals - Manufacturing Technology 73 (2024) 377–380

Contents lists available at ScienceDirect

CIRP Annals - Manufacturing Technology

journal homepage: https://www.editorialmanager.com/CIRP/default.aspx

Predictive digital twin-driven dynamic error control for slow-tool-servo ultraprecision diamond turning

Xichun Luo*, Qi Liu, Abhilash Puthanveettil Madathil, Wenkun Xie

Centre for Precision Manufacturing, DMEM, University of Strathclyde, Glasgow, UK

Submitted by W. Brian Rowe (1), Liverpool, UK

ARTICLE INFO

Article history:
Available online 18 May 2024

Keywords:
Accuracy
Digital twin
Dynamic error control

ABSTRACT

A predictive digital twin (DT)-driven dynamic error control approach is presented for accuracy control in high-frequency slow-tool-servo ultraprecision diamond turning processes. An explainable artificial intelligence-enabled real-time DT of the total dynamic error (inside and outside the servo loop) was established using in-line acceleration input data near the tool. A feedforward controller was used to mitigate the total dynamic errors before they came into effect. The machining trials using this approach showed that significant improvement in machining accuracy (87%, surface form accuracy; 95%, phase accuracy with precisions of 0.06 μm and 0.05°), and efficiency (8 times the state-of-the-art) were successfully achieved.

1. Introduction

Driven by the ever-increasing demand for performance enhancement, lightweight and function integration, freeform (i.e. non-rotational symmetric) optics, such as lens arrays, head-up displays and beam shapers, have been widely applied in the green energy, illumination, automotive and aerospace [1]. Slow-tool-servo(STS) is an important low-cost freeform ultraprecision diamond turning technique. It utilizes the machine's Z (in-feed) slide instead of extra fast-tool-servo devices to move the diamond tool, which is synchronized with the rotation of the work spindle and linear motion of the machine's X (feed) slide, to obtain freeform optics with large sags in millimeter scales. However, STS suffers from low bandwidth of control of the motion (< 5 Hz) and a long cycle time. To achieve the same level of operational frequency as diamond turning of rotationally symmetric optics, typically 10-50 Hz, a significant number of dynamic errors will be generated. The challenge of accuracy control in STS under extremely high operational frequency is considerable, requiring a new effective dynamic error control approach. Addressing this problem was a key motivation for this paper.

In STS, dynamic error is the deviation between the tool and the reference (setpoint) displacements. It includes both servo response (following) errors and mechanical deviations associated with the dynamic response of mechanical structures and interfaces, (i.e., dynamic errors inside and outside the servo loop) [2]. Researchers have developed zero phase error tracking [3], adaptive disturbance discrete-time sliding mode [4] and optimal controllers [5], or pre-compensation of servo tracking errors through data-based reference trajectory modification [6] to reduce tracking errors. Both pre-measurement [7] or model-based error compensation [8]/feedback control [9] approaches have been used to reduce dynamic errors outside the servo loop. However, a systematic approach to mitigate the total dynamic errors, both inside and outside the servo loop, simultaneously is still required.

Emerging digital twin (DT) technology provides a potential solution, as it can digitally reproduce the physical behaviors of machine tools [10] and has been used to predict tracking errors [11] and thermal error compensation [12]. Currently, theoretical or numerical models with a series of hypotheses are usually used to establish a DT, mainly for repeatable errors. The challenge lies in fast processing and the best use of sensor input data, establishing an accurate DT of total dynamic error in real time and realizing effective error control actions.

This paper proposes a novel predictive DT-driven dynamic error control approach that uses acceleration signal inputs, combining explainable artificial intelligence (XAI)-enabled DT and a feedforward controller, to mitigate total dynamic error, not only repeatable systematic errors, but also stochastic errors, before they come into effect in STS ultraprecision diamond turning processes. The significantly improved machining accuracy and efficiency are demonstrated through STS machining trials.

2. Methodology

As shown in Fig. 1, the predictive DT-driven dynamic error control approach was realized by a new control system, including an accelerometer mounted near the tool center position (TCP), an XAI-enabled DT of total dynamic error, and a DT-driven feedforward controller.

* Corresponding author.
E-mail address: xichun.luo@strath.ac.uk (X. Luo).

https://doi.org/10.1016/j.cirp.2024.04.080

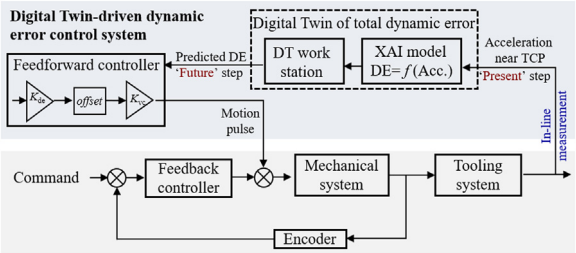

Fig. 1. Concept of the proposed DT-driven dynamic error control approach.

The system was integrated into the servo loop of the CNC control system of the diamond turning machine.

The accelerometer provided acceleration data obtained near the TCP in the present step, including repeatable systematic and stochastic error elements, which couldn't be measured by the machine encoder, as inputs to establish the predictive DT of the total dynamic error at the TCP in the future step.

The prediction of future dynamic error (DE) was made through an XAI model which was presented as a function of acceleration (i.e. *f (Acc)*) near the TCP. The XAI model was trained and calibrated by using data obtained in an offline dynamic error measurement test, which included total dynamic error measurement data and acceleration data, measured by a high-accuracy capacitance sensor mounted at the TCP and a relatively low-accuracy accelerometer mounted near the TCP respectively.

This offline modelling approach mitigates the problem caused by time delays, drift and high noise occurring in conventional double-integration calculation from acceleration to displacement. It empowers the offline-trained XAI model to have high accuracy and real-time computational efficiency. An accurate real-time DT of the total dynamic errors, inside and outside the servo loop, was then established in a DT workstation for practical STS operation.

The feedforward controller took the inputs of the predicted total dynamic error data from the DT and transformed them into voltage signals. To avoid a large step change in the voltage signals, an offset voltage was specified for subtraction from the analogue input value before it was used. The motion pulse was finally generated based on the CNC control system's default voltage and pulse ratio and acted in the servo loop to mitigate the total dynamic errors at the TCP before they came into effect.

Ensuring the overall accuracy of the approach necessitates controlling the uncertainties from sensor noise, XAI modelling simplification and machining environment. These were kept in check through rigorous calibrations, validations and maintaining a controlled machining environment.

3. Measurement of total dynamic error

In STS machining, the periodical tool path can be decomposed into a number of sinusoidal motions of different frequencies (ω) and amplitudes (A) through discrete Fourier transformation. Z axis is the most critical axis as it constantly experiences excessive acceleration and deceleration. To simplify the measurement test, the diamond tool was actuated by the Z axis under a sinusoidal motion command with the motion time (t), which is described as:

$$Z = A * \sin(2\pi * \omega * t) \quad (1)$$

The control bandwidth of the Z-axis was identified as 50 Hz through modal test. Thus, the frequency ω in the test varied from 1, 5 to 40 Hz (for safety reason) with a step of 5 Hz; while amplitude A varied from 1 to 11 μm with a step of 1 μm.

The dynamic error measurement test was performed on a three-axis ultraprecision diamond turning machine equipped with an Aerotech A3200 CNC controller (see Fig. 2a). A capacitance sensor (IBS CP8.0-2.0-2.0) and an accelerometer (PCB 356B) were mounted at the TCP and near the TCP respectively (see Fig. 2a). The capacitance sensor was set up within its working distance against a diamond

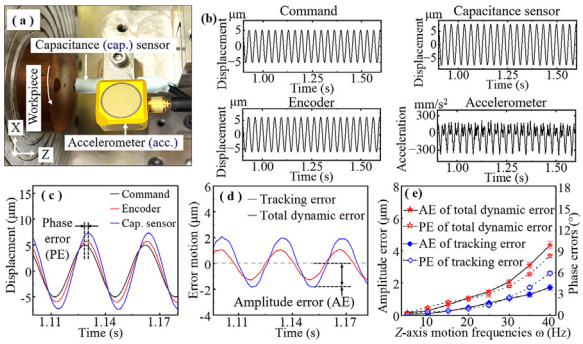

Fig. 2. (a) Experimental set-up; (b) Examples of measured displacements and accelerations; (c) An example of measured displacements by encoder and capacitance sensor; (d) Dynamic errors; (e) Measured amplitude and phase errors at different frequencies.

turned flat copper surface mounted on the machine vacuum chuck to measure the total dynamic error including both tracking error and mechanical structure deformation, which cannot be measured by the machine encoder. The total dynamic error data and the acceleration data collected synchronously by the accelerometer (see Fig. 2b) were used to train and calibrate the XAI prediction model in Section 4.

Fig. 2c shows when A and ω were set as 5 μm and 30 Hz respectively the amplitudes of the sinusoidal displacements measured by the encoder and the capacitance sensor increased to 5.74μm and 7.29μm, while phase errors were 1.06° and 4.13°, respectively. Fig. 2d illustrates the tracking error and the total dynamic errors also possessed sinusoidal forms with amplitudes of 1.06μm and 1.97μm respectively. Fig. 2e illustrates both amplitude and phase errors increased with the increase of operational frequency. As ω increased from 5Hz to 40Hz, the amplitude error and phase error increased from 0.12μm to 4.35μm, and from 0.42° to 8.41°, respectively. Under a frequency of 40Hz, the total dynamic error was nearly three times the tracking error (1.49μm), while its maximum phase error reached 8.56°.

4. DT- driven dynamic error control

4.1. XAI prediction model for total dynamic error

The proposed predictive real-time DT of total dynamic error was based on an XAI prediction model which had a direct numerical correlation between the total dynamic errors and the synchronous acceleration near the TCP. To train and calibrate the XAI model, 99 groups of measured acceleration and dynamic error data were collected with an acquisition time of 6 seconds (t_0 to t_k) for each group in the offline dynamic error measurement test (in Section 3).

As shown in Fig. 3, feature extractions were performed for the acceleration data collected in the first 5 seconds (t_0 to t_n), while the measured capacitance data was used as the ground truth data to calculate the total dynamic error. The extracted 12 features (see Table 1) and calculated dynamic errors constituted the input and output datasets to train the XAI prediction model.

The XAI model was trained based on the PySR algorithm [13], a Python library for symbolic regression in Jupyter v7, which ran in a supervised learning module. The machine learning (ML) model searched in a 12D space for the appropriate function and parameters to map the input-output dataspace.

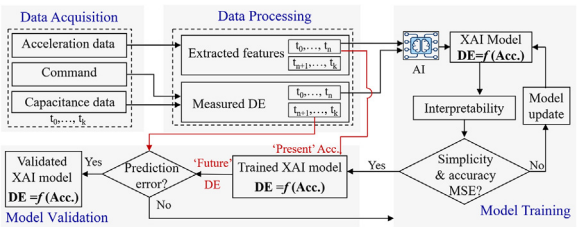

Fig. 3. Methodology to train and calibrate of XAI prediction model.

Table 1
Extracted features from accelerometer signals.

Feature	Label	Feature	Label
Signal frequency	f_1	Skewness	f_7
Mean absolute value	f_2	Crust factor	f_8
Variance	f_3	Impulse factor	f_9
Peak amplitude	f_4	Shape factor	f_{10}
Root mean square	f_5	Mean frequency	f_{11}
Kurtosis	f_6	Total power	f_{12}

The final converged model for the predicted amplitude error in the future time (t_{n+1} to t_k) is described as:

$$DE^{t_{n+1}-t_k}(amplitude) = f(f_1^{t_0-t_n}, f_2^{t_0-t_n}, \ldots, f_{12}^{t_0-t_n}) = 49.67 f_8^{t_0-t_n}\left|\frac{f_3^{t_0-t_n}}{f_5^{t_0-t_n}}\right| \quad (2)$$

which has an excellent predictive performance with an R^2 of 0.989.

Since the overall search space is complex and multi-dimensional, significant dimensionality reduction is required to realize real-time computational efficiency. In this study, the final selected equation had just three features, including variance, crust factor, root mean square (RMS) of the historical (t_0 to t_{n-1}) and present (t_n) accelerometer signals. The acceleration peak and variance represented the maximum inertial forces and jerks respectively during the z-axis motion, aligning with previous studies as some of the prominent causes of dynamic errors [2]. Using them, transparency of the extracted analytic expression would aid in further investigation and remedial actions on the root cause of the dynamic errors.

Meanwhile, the phase error in the future time (t_{n+1} to t_k) was trained based on extracting the difference between the time stamps corresponding to the peak amplitude of the true (capacitance) position and command position signals. It is given by

$$DE^{t_{n+1}-t_k}(phase) = 1.95 - 1.23^{\circ}\tanh(-0.0441 f_1^{t_0-t_n} + 0.122 f_{10}^{t_0-t_n} + 1.08) \quad (3)$$

which has a good predictive performance (R^2 = 0.952).

For calibration, the extracted features of the acceleration data at the present time (t_0 to t_n) were input to the trained XAI model, there obtaining the predicted dynamic error in the future time, which was compared with the measured dynamic error (t_{n+1} to t_k) (see Fig.3). The comparison result shown in Fig. 4a indicates that the XAI predicted dynamic error matched well with the true error measured by the capacitance sensor, with an average prediction error of 68.3 nm. Meanwhile, the XAI models showed an overall R^2 value of 0.987 across all test data (see Fig. 4b), which clearly demonstrated the effectiveness of the XAI model.

Besides, other widely-used ML approaches including Long Short-Term Memory (LSTM) and Nonlinear Autoregressive Neural Network (NARNET) were also adopted for comparison. The statistical results (see Fig. 4c) showed the calculation latency (<0.15s) of the proposed XAI model was significantly smaller than those of LSTM and NARNET while maintaining a similar prediction accuracy (<100 nm), thus underlining the prediction accuracy and efficiency of the proposed XAI model.

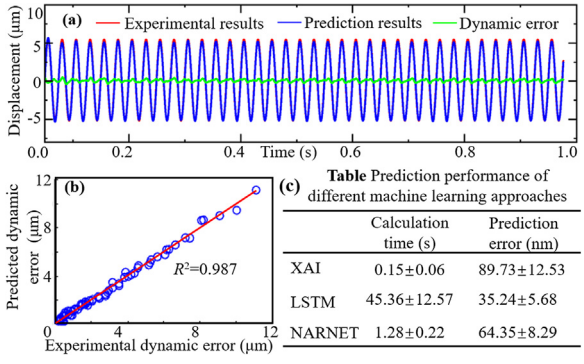

(c) **Table** Prediction performance of different machine learning approaches

	Calculation time (s)	Prediction error (nm)
XAI	0.15±0.06	89.73±12.53
LSTM	45.36±12.57	35.24±5.68
NARNET	1.28±0.22	64.35±8.29

Fig. 4. (a) Model validation; (b) Model performance; (c) Comparison of prediction performance of different ML approaches.

4.2. XAI-enabled real-time DT of total dynamic error

Based on Eqs. (1) and (2), the total dynamic error in the future time (t_{n+1} to t_k) can be calculated as:

$$DE^{t_{n+1}-t_k}(amplitude, phase) = 49.67 f_8^{t_0-t_n}\left|\frac{f_3^{t_0-t_n}}{f_5^{t_0-t_n}}\right|^{0.78} \sin(\omega t_{t_{n+1}-t_k} + \varphi_{t_n} + 1.95 - 1.23^{\circ}\tanh(-0.0441 f_1^{t_0-t_n} + 0.122 f_{10}^{t_0-t_n} + 1.08)) \quad (4)$$

where φ_{t_n} is the motion phase at the current moment.

In order to establish an accurate predictive DT of the total dynamic error in practical STS diamond turning, in-line measured accelerations near the TCP were automatically input to the calibrated XAI prediction model. The high computational efficiency offered by Eq. (4) allowed the real-time calculation of the total dynamic error, thereby, establishing a real-time DT of total dynamic error at the TCP in practical STS diamond turning.

4.3. DT-driven feedforward controller

Taking the inputs from DT of total dynamic error, a feedforward controller was established to automatically generate precision motion pulse signals as motion commands to control the movement of the machine stage and to mitigate machine dynamic errors before they came into action (see Fig.1).

Given the relation between the control voltage and the motion pulses (P) was the default (K_{vc}) in the servo loop, the detailed transformation from the predicted dynamic error (DE_{pre}) to the motion pulse signals was via a pre-defined ratio scale K_{dv} of displacement to voltage, which is expressed as:

$$P = (DE_{pre}/K_{dv} - offset) * K_{vc} \quad (5)$$

where the offset voltage was specified to be subtracted from the analogue input value before it was used, preventing a large step change when the voltage became large.

5. Implementation and evaluation

The implementation of the proposed dynamic error control system for practical STS ultraprecision diamond turning is illustrated in Fig. 5. An accelerometer (PCB 356B) was mounted near the TCP. The XAI-enabled DT of the total dynamic error and the feedforward controller, was implemented in a real-time control prototype machine (Performance, Speedgoat) which possessed state-of-the-art I/O and FPGA modules.

In practical SLS machining, the dynamic error for the future time was forecasted through the XAI-enabled DT prediction model using

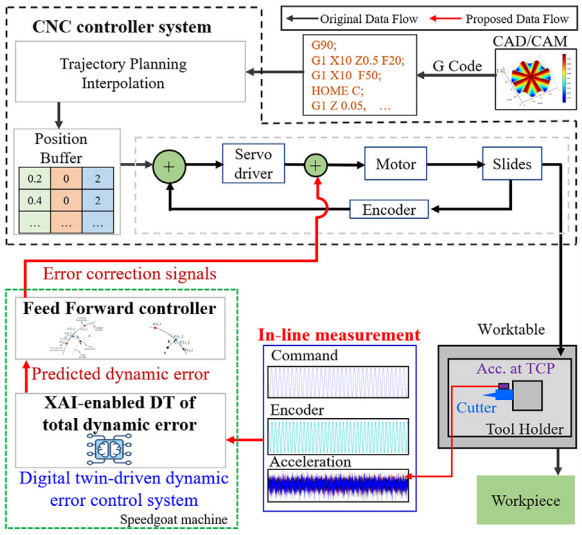

Fig. 5. Implementation of the proposed dynamic error control approach.

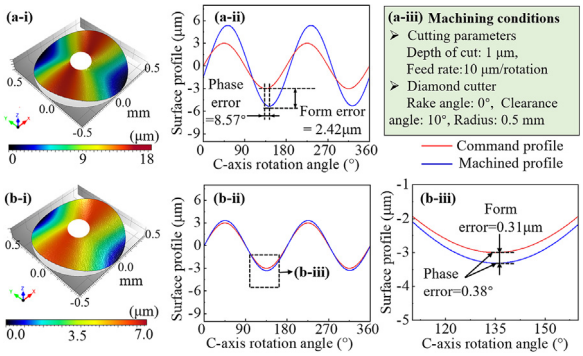

Fig. 6. Measured machined surfaces at 40Hz operational frequency without (a) and with (b) the proposed dynamic error control approach.

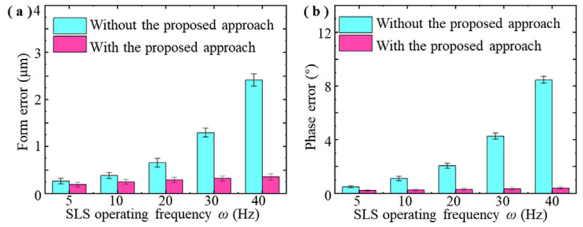

Fig. 7. Comparison of the machined surfaces produced with and without using the proposed dynamic error control approach at different operational frequencies: (a) form error and (b) phase error.

acceleration input data obtained near the TCP and was saved in a buffer. The feedforward controller, built-in MATLAB/Simulink 2022b, was connected to the servo loop of the diamond turning machine's CNC controller through an expanded analogue interface using a customized AeroBasic command in real time. The updating rate for communication was set the same as that of the servo loop of the diamond machine (8kHz).

To evaluate the effectiveness of the approach, a series of STS diamond cutting trials were conducted to generate freeform bicuspid surfaces on copper workpieces, which is described as:

$$z = 0.006 * x * \sin(2C) - 0.006 * x \quad (6)$$

where x is the position of the X axis, and C is the rotation angle of the C axis. The operational frequency was set as 5Hz, 10Hz, 20Hz, 30Hz and 40Hz respectively in machining trials. The machining condition is shown in Fig. 6a.

Fig. 6 presents the measured freeform surfaces machined at 40 Hz with and without applying the proposed dynamic error control approach. Fig. 6a-i shows the machined surface amplitude was 5.48μm against a theoretical value of 3 μm in the area with a radius of 0.5mm from the workpiece centre. This indicates a form error (peak-peak) of 2.42μm. When applying the proposed approach, the surface form error (see Fig. 6b-i) was significantly reduced to 0.31μm, indicating up to 87% dynamic error has been mitigated under an operational frequency of 40 Hz. The phase error was reduced from 8.57° (see Fig. 6a-ii) to 0.38° (see Fig. 6b-iii). It means the proposed dynamic error control approach allowed operating STS machining at an extremely high frequency (8 times of the state-of-the-art) without comprising required accuracy.

Fig. 7 depicts the measured form and phase errors of the machined surfaces at different operational frequencies with and without applying the proposed dynamic error control approach. Significant improvement in both surface form (up to 87%) and phase accuracies (up to 95%) with precisions up to 0.06μm and 0.05° were consistently realized. Moreover, the efficiency of the STS machining was dramatically improved. This effectiveness of the dynamic error control approach in accuracy control has therefore been fully demonstrated.

6. Conclusion

This paper presented a predictive DT-driven dynamic error control approach implemented in a Speedgoat real-time control prototype machine for accuracy control in high-frequency STS ultra-precision diamond turning. Based on an XAI prediction model, pre-trained and calibrated by sensor data obtained through a dynamic error measurement test, a real-time DT of the total dynamic error (inside and outside the servo loop) was successfully established using in-line measured acceleration input data near the TCP in practical STS operation, considering both repeatable systematic and stochastic error elements. The established DT-driven feedforward controller was able to mitigate dynamic errors before they came into effect. The machining trials show that significant improvements in machining accuracy (87%, surface form accuracy; 95%, phase accuracy with precisions of 0.06μm and 0.05°) and efficiency (8 times state-of-the-art) were successfully achieved when applying this approach.

To make the proposed approach industrially viable for other production processes, training of the XAI model considering emulated cutting forces and crosstalk of dynamic error of multiple axes will be performed in the future.

Declaration of competing interest

The authors declare that they have no known competing financial interests or personal relationships that could have appeared to influence the work reported in this paper.

CRediT authorship contribution statement

Xichun Luo: Writing – review & editing, Writing – original draft, Supervision, Resources, Project administration, Methodology, Funding acquisition, Conceptualization. **Qi Liu:** Writing – review & editing, Writing – original draft, Visualization, Validation, Software, Methodology, Investigation, Formal analysis, Data curation. **Abhilash Puthanveettil Madathil:** Writing – review & editing, Writing – original draft, Visualization, Validation, Software, Methodology, Investigation, Formal analysis, Data curation. **Wenkun Xie:** Writing – review & editing, Writing – original draft, Visualization, Methodology.

Acknowledgments

The authors would like to thank EPSRC (EP/K018345/1, EP/T024844/1, EP/V055208/1), Dr. Simon Smith and Dr. Chris Charlesworth of Aerotech Ltd for supporting this research.

References

[1] Fang F-Z, Zhang X-D, Weckenmann A, Zhang G-X, Evans C (2013) Manufacturing and Measurement of Freeform Optics. *Annals of the CIRP* 62(2):823–846.
[2] Lyu D, Liu Q, Liu H, Zhao W (2019) Dynamic Error of CNC Machine Tools: A State-Of-The-Art Review. *Int J Adv Manuf Technol* 106(5-6):1869–1891.
[3] Tomizuka M (1987) Zero Phase Error Tracking Algorithm For Digital Control. *ASME Trans J Dyn Syst Meas Control* 109(1):65–68.
[4] Okwudire C, Altintas Y (2009) Minimum Tracking Error Control of Flexible Ball Screw Drives Using a Discrete-Time Sliding Mode Controller. ASME Trans J Dyn Syst Meas Control 131:0510.
[5] Sencer B, Dumanli A (2017) Optimal Control Of Flexible Drives With Load Side Feedback. *Annals of the CIRP* 66(1):357–360.
[6] Dumanli A, Sencer B (2019) Pre-Compensation Of Servo Tracking Errors Through Data-Based Reference Trajectory Modification. *Annals of the CIRP* 68(1):397–400.
[7] Morantz P, Luo X, Shore P (2007) Characterisation of Dynamic Errors Of An Ultra Precision Machine Tool. In: *Proceedings of the 8th LAMDAMAP International Conference*, Cardiff4–13.
[8] Huang H-W, Tsai M-S, Huang Y-C (2018) Modeling and Elastic Deformation Compensation Of Flexural Feed Drive System. *Int J Mach Tools Manuf* 132:96–112.
[9] Huynh H-N, Altintas Y (2022) Multibody Dynamic Modeling Of Five-Axis Machine Tool Vibrations And Controller. *Annals of the CIRP* 71(1):325–328.
[10] Bergs T, Biermann D, Erkorkmaz K, M'Saoubi R (2023) Digital Twins for Cutting Processes. *Annals of the CIRP* 72(2):541–567.
[11] Kim H, Okwudire C E (2023) Intelligent Feedrate Optimization Using a Physics-Based and Data-Driven Digital Twin. *Annals of the CIRP* 72(1):325–328.
[12] Irino N, Kobayashi A, Shinba Y, Kawai K, Spescha D, Wegener K (2023) Digital Twin Based Accuracy Compensation. *Annals of the CIRP* 72(1):345–348.
[13] Cranmer, M (2023) Interpretable Machine Learning for Science with PySR and SymbolicRegression.jl. https://arxiv.org/abs/2305.01582v3 (accessed 9/3/24).